Available online at www.sciencedirect.com
ScienceDirect
Applied Catalysis B: Environmental 78 (2008) 210–221
APPLIED CATALYSIS B: ENVIRONMENTAL
www.elsevier.com/locate/apcatb

A new concept in high performance ceria–zirconia oxygen storage capacity material with Al_2O_3 as a diffusion barrier

Akira Morikawa [a,*], Tadashi Suzuki [a], Takaaki Kanazawa [b], Koichi Kikuta [c], Akihiko Suda [a], Hirofumi Shinjo [a]

[a] *Catalyst Lab., Toyota Central R&D Labs., Inc., 41-1 Yokomichi, Nagakute, Nagakute-Cho, Aichi-Gun, Aichi 480-1192, Japan*
[b] *Toyota Motor Co. Ltd., Catalyst Design Dept., Mat. Eng. Div. 1, 1 Toyota-Cho, Toyota, Aichi 471-8572, Japan*
[c] *Nagoya University, Graduate School of Engineering, Department of Crystalline Materials Science, Furo-Cho, Chikusa-ku, Nagoya, Aichi 464-8603, Japan*

Received 27 February 2007; received in revised form 31 August 2007; accepted 12 September 2007
Available online 19 September 2007

Abstract

CeO_2–ZrO_2 solid solution ((Ce,Zr)O_2) is an indispensable oxygen storage capacity (OSC) material for emission control in gasoline-fuelled automobiles. The high performance OSC material developed in this study is composed of Al_2O_3 as ''a diffusion barrier'' and (Ce,Zr)O_2 particles in intervening layers on a nanometer scale, and is abbreviated as ''ACZ''. The Brunauer–Emmett–Teller (BET) specific surface area (SSA) of ACZ after durability testing in air at 1000 °C was 20 m^2/g, which is higher than that of conventional CZ (2 m^2/g) composed of (Ce,Zr)O_2 without Al_2O_3. After heat treatment at 1000 °C in air, the particle size of (Ce,Zr)O_2 in ACZ was about 10 nm and that without Al_2O_3 was one-half of the size in pure CZ. The OSC was roughly characterized by the total capacity (OSC-c1) and the oxygen release rate (OSC-r). In a fresh catalyst, ACZ and CZ had almost the same OSC-c1; however, the OSC-r of ACZ was twice as fast as CZ. After durability testing, the OSC-r of both ACZ and CZ were reduced significantly, but the OSC-r of ACZ was about five times as fast as CZ. While the OSC-c1 was hardly influenced by the (Ce,Zr)O_2 crystallite size and Pt particle size on the supports, the OSC-r was influenced by both of these parameters. The improvement of the OSC-r in the fresh catalyst and inhibition of the decrease in the OSC-r after durability testing were achieved by suppression of particle growth of (Ce,Zr)O_2 in ACZ by introducing Al_2O_3 as a diffusion barrier with resultant inhibition of sintering of Pt particles.

Keywords: Al_2O_3; CeO_2; ZrO_2; Diffusion barrier; Oxygen storage capacity

1. Introduction

1.1. Background and aim

The three-way catalysts for gasoline-fuelled automobiles can simultaneously remove the three components – CO, HC (hydrocarbons), and NO_x – most efficiently at the theoretical air/fuel (A/F) ratio of around 14.6 [1]. A ceria–zirconia solid solution is an indispensable material to maintain the A/F ratio precisely at the catalyst surface by a function of ''oxygen storage capacity,'' (OSC) which originates in the valence change between Ce^{4+} and Ce^{3+} and has been developed by various automotive companies [2,3]. Recently, emission regulations, such as EURO5, LEVII, and J-SULEV, introduced in every country in the world from the second half of the 1990s, are more severe than earlier regulations. As a result of these tightened regulations, fuel combustion had to be more precisely controlled, resulting in higher temperature of emission. In order to adapt to the higher temperatures, improvement in the performance and durability of the ceria–zirconia solid solution is required [4–10]. ACZ is a term used for the composite of alumina (A) and ceria–zirconia solid solution (Ce,Zr)O_2 (CZ) on a nanometer scale, which was practically applied in three-way catalysts as OSC material in 2001 [4]. The concept of introducing alumina into ceria–zirconia solid solution on a nanometer scale was named the ''diffusion barrier concept''. The three-way catalysts containing ACZ have successfully purified automotive toxic emissions in initial (fresh) conditions and have been able to maintain their performance throughout

* Corresponding author. Tel.: +81 561 61 4792; fax: +81 561 63 6150.
E-mail address: a-morikawa@mosk.tytlabs.co.jp (A. Morikawa).
URL: http://www.tytlabs.co.jp/eindex.html

0926-3373/$ – see front matter © 2007 Elsevier B.V. All rights reserved.
doi:10.1016/j.apcatb.2007.09.013

the life of the car. Though attempts to understand the basic properties of ACZ have been made [4], [24,25], the reason why ACZ has such an excellent heat resistance and a high OSC is still unclear because these studies were fragmentary and not quantitative. Particularly, the studies of OSC from the view point of oxygen release rate were hardly performed in spite of the importance. Additionally, it is not clear whether the Al_2O_3 diffusion barrier must be introduced not at the micron or submicron scale but at the nanometer scale. Understanding these properties would provide some important information to improve the performance of OSC materials targeting the next-generation. The purpose of this research is to clarify the effect of introducing alumina into ceria–zirconia solid solution as a diffusion barrier on the physical properties and OSC characteristics, especially oxygen release rate, in order to obtain the guiding principles for developing next-generation OSC materials.

1.2. The concept of "diffusion barrier"

This concept was reported in our earlier study [4]. A schematic diagram of this concept is shown in Fig. 1. Generally, it is thought that growth of $(Ce,Zr)O_2$ nano-particle is generated by contact of the primary particles [11]. In this case, if another oxide that does not react with $(Ce,Zr)O_2$ in solid phase is introduced into $(Ce,Zr)O_2$ on a nanometer scale, the contact of $(Ce,Zr)O_2$ primary particles is restricted and growth of the particles could be inhibited.

2. Experimental

2.1. Preparation of ACZ

ACZ was prepared by the co-precipitation method. First, an aqueous salt solution containing 1 M $Al(NO_3)_3{\cdot}9H_2O$ (Wako Pure Chemicals), 0.5 M $Ce(NO_3)_3{\cdot}6H_2O$ (Wako), and 0.5 M $ZrO(NO_3)_2{\cdot}2H_2O$ (Wako) was prepared. Then, hydrogen peroxide of 1.1 times the amount of cerium was added to the salt solution as an aqueous solution (25 wt%, Wako). Next, the salt solution after stirring was added to an ammonium hydroxide solution (25 wt%, Wako) containing ammonia of 1.2 times the concentration corresponding to a neutralization equivalent for the salt solution, and then a mixed hydroxide precursor was obtained. After centrifugal separation of the obtained precursor, the supernatant liquid was removed from the precipitated precursor. This separation process was repeated twice using ion exchange water. The precursor was dried for 3 h at 110 °C in air. The dried precursor was calcinated in two steps in air. The first step was carried out at 400 °C for 5 h, and in the second step, calcination was performed at 700 °C for 5 h after which a final material was obtained. The relative proportions of each constituent in ACZ were $Al_2O_3/CeO_2/ZrO_2 = 1:1:1$ (mol ratio). Two samples were selected as comparative materials. The first was CZ, which was composed of only a ceria–zirconia solid solution and was prepared similar to ACZ without adding the alumina source. The relative proportions of each constituent in CZ were $CeO_2/ZrO_2 = 1:1$ (mol ratio). The second comparative sample was CZ + Al_2O_3 composed of CZ prepared as mentioned above and mixed with Al_2O_3 in a mortar.

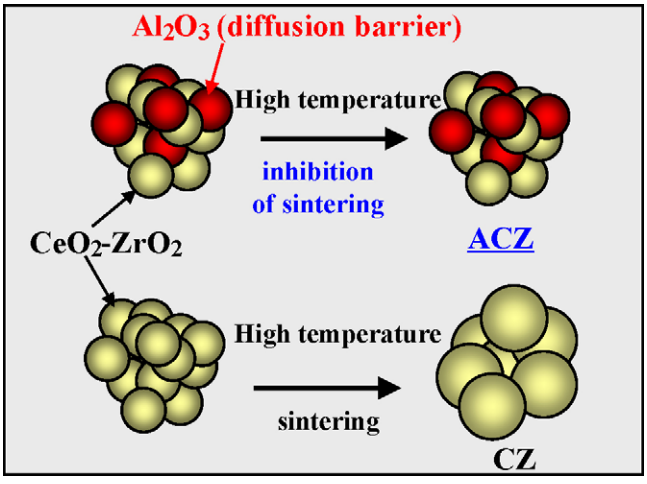

Fig. 1. Illustration of "diffusion barrier concept".

2.2. Pt loading on ACZ

Platinum (2 wt%) was loaded on ACZ and CZ by the impregnation method of $Pt(NO_2)_2(NH_3)_2$ solution (Tanaka Noble Metals Co. Ltd.). Both Pt loaded powders were calcinated at 300 °C for 3 h in air. The obtained catalyst powders were compressed with a cold isostatic press (CIP) apparatus under 100 MPa, and the compressed block was broken into catalytic pellets of diameter from 0.5 to 1 mm. In the later sections, these fresh catalysts are abbreviated as PtACZ(F) and PtCZ(F). Moreover, to compare the catalytic properties, aged ACZ and CZ were fabricated by thermal treatment at 1000 °C for 5 h in air. After this heat treatment, Pt was loaded on ACZ or CZ by the impregnation process as discussed above. Each of these catalysts is abbreviated as PtACZ(P) and PtCZ(P).

2.3. Durability test of catalysts

The catalysts, PtACZ(F) and PtCZ(F), were loaded into separate quartz crucibles, and were set in the furnace. The durability test was performed under conditions shown in Table 1. The catalysts are abbreviated as PtACZ(A) and PtCZ(A).

2.4. Brunauer–Emmett–Teller (BET) specific surface area measurement

BET specific surface areas of ACZ, CZ, and CZ + Al_2O_3 before and after durability testing were measured by the

Table 1
Durability-test conditions

Atmosphere	Air
Catalyst weight	3 g
Soaking temperature	1000 °C
Soaking time	5 h

Table 2
Conditions for BET specific surface area measurement

Pre-treatment atmosphere	Pure nitrogen gas
Pre-treatment temperature	200 °C, 15 min
Pre-treatment gas flow rate	25 ml/min per reaction pipe
Adsorption gas	N_2 (30%)/He balance
Adsorption gas flow rate	25 ml/min per reaction pipe
Adsorption temperature	−196 °C (in liquid nitrogen)

BET one-point method under conditions shown in Table 2 using the Micro-Data automatic surface area analyzer (model-4232II).

2.5. X-ray diffraction analysis

Diffraction patterns of ACZ, CZ, and CZ + Al_2O_3 were measured before and after durability testing at diffraction angles (2-θ) from 20 to 70° using RINT-TTR X-ray diffraction apparatus (RIGAKU Corporation). The conditions for measurement are shown in Table 3. Crystal phases of the ceria–zirconia solid solution were identified, and the diameters of crystallite particles were calculated from full width at half maximum of (1 1 1) lattice planes according to Scherrer's equation.

2.6. TEM observation

TEM observation of ACZ, CZ, and CZ + Al_2O_3 was carried out using field emission transmission electron microscopy (FE-TEM) using a Hitachi HF-2000 with an energy dispersive X-ray (EDX) analyzer.

2.7. Pt size measurement by CO pulse adsorption method

Pt size in the catalysts before and after durability testing was measured using a CO pulse adsorption apparatus (Okura Riken Co. Ltd.). After pre-treatment under conditions recommended by the Catalysis Society of Japan [12,13], catalysts were cooled in a dry ice/ethanol bath, and measurements were carried out at about −70 °C [14]. The measurement conditions are shown in Table 4.

2.8. OSC evaluation method

OSC is roughly classified into two types. The first is the quantity of all releasable oxygen in a specimen that can react with a reducing agent (e.g., CO, H_2) at a pre-determined temperature, which is called "OSC-c". The second is the desorption rate of oxygen, which is called "OSC-r".

Table 3
XRD measurement conditions

X-ray source	Cu K-alpha 1
Measurement condition	50 kV, 300 mA
Scanning range (2-θ)	20–70°
Scanning rate (2-θ)	2° min^{-1}

Table 4
Measurement conditions of Pt dispersion and Pt particle size

Pre-treatment process	
Atmosphere	O_2 (100%) → He carrier → H_2 (100%) → He carrier
Temperature	400 °C
Time	Each step for 15 min
Measurement process	
Atmosphere	He carrier
CO pulse size	0.7 μmol per pulse
Temperature	−70 °C in dryice + ethanol
Common condition	
Amount of catalysts	0.2 g
Total flow rate	20 ml/min

2.8.1. Saturated "OSC-c" measurement

OSC-c was measured by the following method [15]. The 2 wt% Pt loaded CZ catalyst was placed in a thermogravimetric analyzer and was pre-treated at 500 °C for 15 min under an O_2 (20%)/N_2 (balance) atmosphere. After the pre-treatment, it was cooled to 300 °C under the same oxidative atmosphere. After reaching the pre-determined temperature, the atmosphere was changed from O_2 (20%)/N_2 (balance) to H_2 (20%)/N_2 (balance), and these conditions were retained until weight reduction in the catalyst was no longer detected. Subsequently, the atmosphere was changed to O_2 (20%)/N_2 (balance) again, and the atmosphere and temperature were maintained until the weight increase in the catalyst was no longer detected. These steps were repeated until the weight reduction under H_2 (20%)/N_2 (balance) and the weight increase under O_2 (20%)/N_2 (balance) became almost the same value reversibly; subsequently, an additional two cycles were repeated. Then, the averages of each weight reduction and increase were calculated. The saturated OSC was indicated in two ways. The saturated OSC-c1 was denoted as the amount of O_2 adsorption/desorption per unit weight of catalyst [(O_2) μmol/(catalyst) g]. The saturated OSC-c2 [9,10] was denoted as the amount of O_2 adsorption/desorption per mol of CeO_2 contained in a catalyst [(O_2) mol/(CeO_2) mol], which became a dimensionless quantity; because CeO_2 content per unit catalyst weight differed for each sample.

2.8.2. Measurement of oxygen release rate (OSC-r)

In this research, oxygen release rate (OSC-r) was evaluated by measuring the amount of CO_2 formation under a dynamic atmosphere where CO and O_2 were introduced into a catalyst every 3 min. A fixed bed flow-type reaction apparatus was used for this evaluation, which followed the experiment conducted by Tanabe et al. [16]. Measurement conditions are shown in Table 5.

A flow-type reactor is usually used for measuring general catalytic activity. The apparatus used in this evaluation had a structure in which injectors were attached near the gas mixing point, which was capable of supplying CO and O_2 to a catalyst without mixing the gases on the catalyst. In this reaction apparatus, by mixing CO and O_2 with N_2 carrier gas, CO/N_2 (balance) and O_2/N_2 (balance) of pre-determined concentra-

Table 5
Measurement conditions of oxygen release rate

Resource of each gas	
Injection gas for oxidation atmosphere	O_2 (50%)/N_2 balance
Injection gas for reduction atmosphere	CO (100%)
Career gas	N_2
Composition of gas that passed catalysts	
Oxidation gas	O_2 (1%)/N_2 balance
Reduction gas	CO (2%)/N_2 balance
Flow time of oxidation gas	180 s
Flow time of reduction gas	180 s
Flow rate	5 L/min
Amount of catalysts	1 g
Pre-treatment conditions	500 °C, 18 min
Measurement condition	300 °C, 30 min
Detector	
CO, CO_2	Non-dispersive infrared spectrophotometer (ND-IR)
O_2	Magnetic oxygen analyzer

tions were supplied to a catalyst. In this method, since CO or O_2 was not simultaneously supplied to a catalyst, CO was oxidized to CO_2 only by the oxygen supplied from the catalyst. In this case, the amount of CO_2 generated according to the reaction on the catalyst was integrated and this value was converted to the amount of oxygen emitted from a catalyst, and the saturated OSC of a catalyst could be calculated from the total integrated value at the measurement temperature. Moreover, in order to obtain the OSC of the time domain of the second unit, it was assumed that the variation of CO_2 generated from 0 s, when the reaction gas was changed from O_2 to CO and started to generate CO_2, to 5 s was almost constant. In this case, the gradient of the tangential line to the CO_2 production curve was the amount of oxygen released per unit time and was expressed as OSC-r (Fig. 2).

3. Results and discussion

3.1. Specific surface area (SSA)

The specific surface areas of CZ, CZ + Al_2O_3 and ACZ after heat treatment at each temperature is shown in Fig. 3. The specific surface area of ACZ was twice as large as that of CZ at 700 °C (initial condition). In addition, ACZ maintained a higher specific surface area than CZ after each heat treatment; for example, after heat treatment at 900 °C, the specific surface area of ACZ was 40 m^2/g (that of CZ was below 2 m^2/g). After heat treatment at 1000 °C, ACZ had a specific surface area of 20 m^2/g but that of CZ was below 1 m^2/g. The specific surface areas of CZ + Al_2O_3 were approximately intermediate between those of the other two catalysts at each temperature.

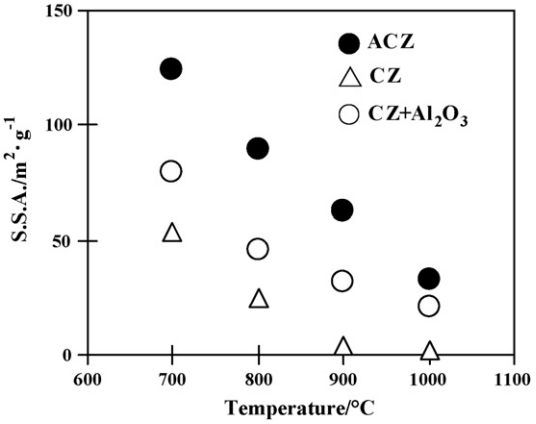

Fig. 3. Specific surface areas (SSA) of CZ, CZ + Al_2O_3, and ACZ after heat treatment from 700 °C (fresh) to 1000 °C in air.

3.2. XRD

The crystallite size of (Ce,Zr)O_2 solid solution was calculated from Scherrer's equation for the full width at half maximum of the XRD profiles of CZ, CZ + Al_2O_3, and ACZ powders, which were fresh and heat-treated at 1000 °C as shown in Fig. 4. The profiles of fresh CZ, CZ + Al_2O_3, and ACZ were almost the same, and these patterns were assigned to a single phase of uniform (Ce,Zr)O_2 solid solution that had the same Ce/Zr ratio as that of the mixture of raw materials [17]. In addition, only in the case of CZ + Al_2O_3 was a peak identified as gamma Al_2O_3 detected.

The crystallite sizes of (Ce,Zr)O_2 solid solution of fresh CZ, CZ + Al_2O_3, and ACZ were each between 6 and 8 nm, and there was no significant difference among these samples.

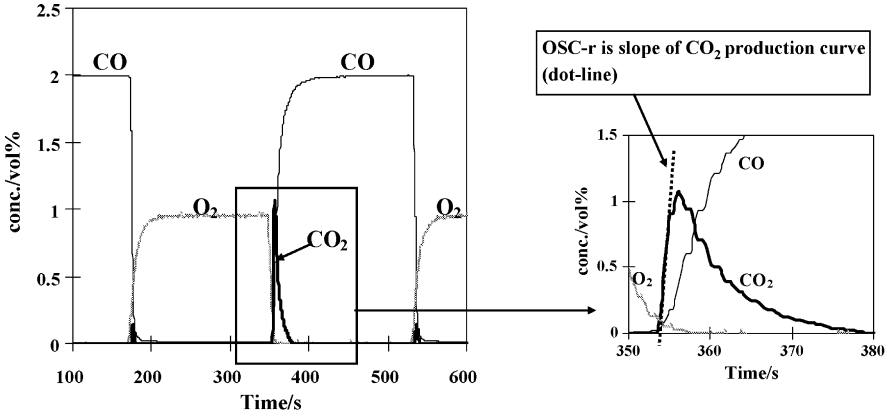

Fig. 2. Evaluation of initial oxygen released rate (OSC-r).

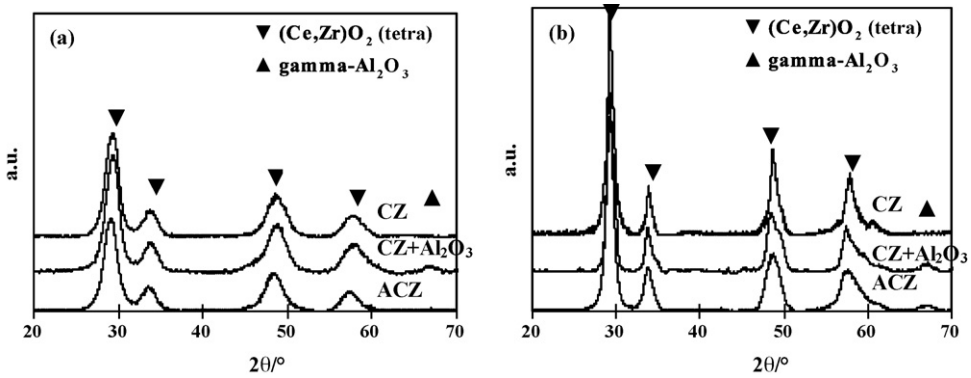

Fig. 4. XRD profiles of CZ, CZ + Al_2O_3, and ACZ for (a) fresh and (b) after heat treatment at 1000 °C in air. (tetra) indicates a tetragonal t″-phase [26].

After heat treatment at 1000 °C, the crystallite size of the $(Ce,Zr)O_2$ solid solution in CZ increased to about 20 nm as shown in Fig. 5, which was about two times larger than that of fresh CZ. Also, the crystallite size of $(Ce,Zr)O_2$ in CZ + Al_2O_3 was increased to about 20 nm. On the other hand, the size of crystallites in ACZ heated at 1000 °C was only about 10 nm as shown in Fig. 5. Sintering of $(Ce,Zr)O_2$ in ACZ resulted in solid solution crystallites of one-half the size of those in CZ and CZ + Al_2O_3.

Moreover, in heated ACZ, a weaker peak than that in CZ + Al_2O_3 ascribed to alumina was observed.

3.3. TEM observation

The results of TEM observations of CZ, CZ + Al_2O_3, and ACZ after heat treatment at 1000 °C are shown in Figs. 6–8. The sizes of secondary particles in CZ, CZ + Al_2O_3, and ACZ in submicron scale are shown in Figs. 6a, 7a and 8a, respectively.

From the results of the EDX analysis, it was found that the secondary particles in CZ contained only Ce and Zr atoms as shown in Fig. 6b and Table 6. This result indicated that the primary particles of $(Ce,Zr)O_2$ around 20 nm had agglomerated and the dense secondary particles were composed. In the case of CZ + Al_2O_3, the EDX result indicated that this sample was composed of secondary particles of CZ and Al_2O_3 mixed at the submicron scale as shown in Fig. 7 and Table 7.

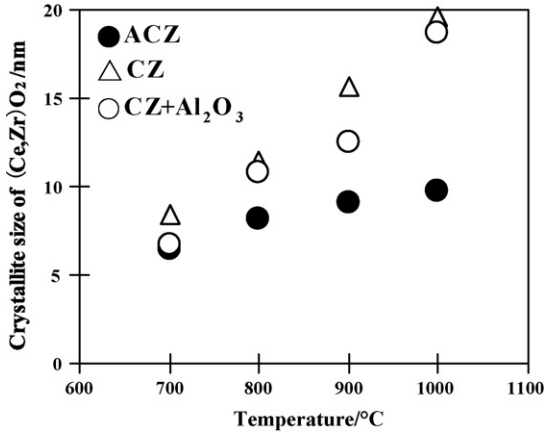

Fig. 5. Crystallite size of $(Ce,Zr)O_2$ solid solution after heat treatment from 700 °C (fresh) to 1000 °C in air.

On the other hand, in ACZ, all of the Al, Ce, and Zr constituents were detected simultaneously at each analysis point in EDX. Since the TEM analysis was performed using a transmission electron beam and information on the depth direction of the samples was usually extracted, it was difficult to detect the signal only concerning either Al or the sum of Ce and Zr. Then, the diameters of the analysis spots were narrowed down to the smallest size (about 1 nm) and the relative amount of Al and the sum of Ce and Zr within the view of each analysis spot was evaluated. If the Al portion of the spot was higher than that of the average of the entire view (spot No. 21 in Fig. 8b, Table 8), the particle was identified as Al_2O_3, and if it was less than that of the average, the analysis spot was identified as a $(Ce,Zr)O_2$ particle. For example, spot Nos. 22 and 24 in Fig. 8b were identified as Al_2O_3 and Nos. 23 and 25 were recognized as $(Ce,Zr)O_2$.

Consequently, it turned out that ACZ consisted of an alternating nanostructure of primary particles of Al_2O_3 (red analysis points in Fig. 8b and $(Ce,Zr)O_2$ (yellow analysis points in Fig. 8b, and the size of $(Ce,Zr)O_2$ was about 10 nm.

3.4. Discussion of physical properties

As shown in Fig. 3, after heat treatment including the fresh catalyst at any temperature, the specific surface area of ACZ was larger than that of CZ and CZ + Al_2O_3. ACZ contains Al_2O_3 as one constituent. Compared with CeO_2 or ZrO_2, the molecular weight of Al_2O_3 is smaller and its surface area per unit mass is larger. This implies the possibility that the high surface area of ACZ may depend on the contribution of the surface area of Al_2O_3 rather than that of $(Ce,Zr)O_2$. This implication must be verified from the relationship between the specific surface area and the crystallite size of $(Ce,Zr)O_2$ in CZ and ACZ computed by XRD measurement as shown in Fig. 5. The crystallite size of $(Ce,Zr)O_2$ in CZ, CZ + Al_2O_3, and ACZ fresh powders were almost equivalent; therefore, the contribution of Al_2O_3 particles to the specific surface area is predominant in fresh samples.

On the other hand, in ACZ, after heat treatment at 1000 °C, the crystallite size of $(Ce,Zr)O_2$ was about one-half of that in

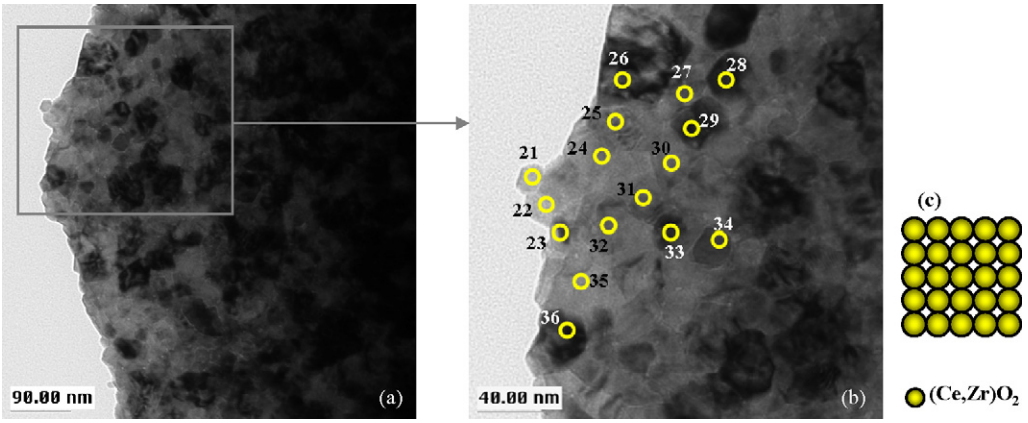

Fig. 6. TEM image of CZ after heat treatment at 1000 °C in air for (a) low magnification, (b) large magnification for square frame in image (a), and (c) the model of secondary particles of CZ.

CZ and CZ + Al_2O_3. This suggests that sintering of $(Ce,Zr)O_2$ in ACZ was restricted by intervening particles of Al_2O_3 not at the submicron scale but at the nanometer scale. CZ has no such obstacles to prevent sintering among particles and CZ + Al_2O_3 has Al_2O_3 particles mixed with $(Ce,Zr)O_2$ particles on the nanometer scale in mortar. Furthermore, each $(Ce,Zr)O_2$ diffraction line was identified to a tetragonal t″-phase, in which cation arrangement showed cubic fluorite structure and only their oxygen arrangement might have less symmetry [26].

According to the TEM image of each sample after heat treatment at 1000 °C, the secondary particles in ACZ consisted of alternating indefinite Al_2O_3 particles and about 10 nm sized $(Ce,Zr)O_2$ particles that were almost the same size as the crystallite size measured by XRD. In contrast, the secondary particles of CZ were only composed of 20 nm primary particles of $(Ce,Zr)O_2$ and those of CZ + Al_2O_3 were composed of secondary particles of CZ and Al_2O_3 mixed on the submicron scale. The sizes of $(Ce,Zr)O_2$ particles in these samples were almost the same as the crystallite size measured by XRD and were twice the size of the $(Ce,Zr)O_2$ particles in ACZ. On the other hand, Al_2O_3 particles were not clearly observed in TEM micrograph. Al_2O_3 usually transforms from gamma phase to theta, delta, or alpha phase after heat treatment at 1000 °C [18,19]. In spite of such a severe level of heat treatment, such a phase transformation of Al_2O_3 was not observed in ACZ after the durability test in Fig. 4. This suggests that the heat-resisting property of Al_2O_3, which is used as a diffusion barrier, is also improved by the presence of $(Ce,Zr)O_2$ in the alternating dispersed as a diffusion barrier for Al_2O_3. Therefore, Al_2O_3 crystallites in ACZ may keep nearly amorphous structure and not apparently be observed in TEM image. Additionally, it is assumed that much larger atomic weight of Ce and Zr than that of Al and highly crystalline of $(Ce,Zr)O_2$ make it difficult to identify the crystallites of Al_2O_3 among those of $(Ce,Zr)O_2$.

These facts suggest that not only the high surface area of Al_2O_3 but also the effect of Al_2O_3 to prevent sintering of $(Ce,Zr)O_2$ primary particles helped maintain the higher specific surface area of ACZ. However, the difference of the specific surface areas between of ACZ and CZ + Al_2O_3 at 1000 °C shown in Fig. 3 was not corresponding to that of the crystallite sizes shown in Fig. 5. That is why the size shown in Fig. 5 were diameters of average crystallite size of $(Ce,Zr)O_2$ in each catalyst measured by XRD. Hence, the changing tendency by heat-treatment of their XRD crystallite size is not corresponding to that by average particle size expected from their specific surface area. Additionally, it should be noticeable phenomenon that the values of 900 °C in Fig. 5 showed the small suppression effect of sintering of $(Ce,Zr)O_2$ in CZ + Al_2O_3.

Furthermore, since no phase other than Al_2O_3 and $(Ce,Zr)O_2$ was observed in the XRD profile of ACZ shown in Fig. 4, it can be said that, there was no solid phase reaction of Al_2O_3 and $(Ce,Zr)O_2$ after heat treatment at 1000 °C in air.

In CZ + Al_2O_3, a phase occurring as a result of reaction of Al_2O_3 and $(Ce,Zr)O_2$ was not observed, but the peak identified as gamma Al_2O_3 phase was sharper than that in ACZ.

This result suggests that two intervening oxides at the nanometer scale inhibit mutual particle growth when they do not react mutually, and that the diffusion barrier is effective.

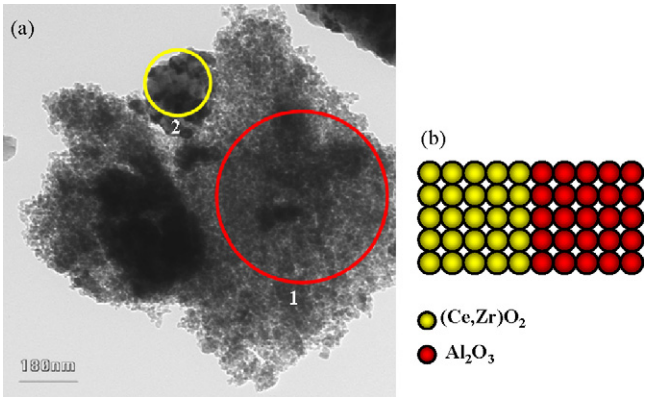

Fig. 7. TEM image of CZ + Al_2O_3 after heat treatment at 1000 °C in air for (a) low magnification and (b) the model of secondary particles of CZ + Al_2O_3.

3.5. OSC characterization

3.5.1. OSC measured by thermogravimetric analyzer

The OSC-c1 of the fresh and aged catalysts is shown in Fig. 9 and Table 9. The measurement was taken after loading Pt

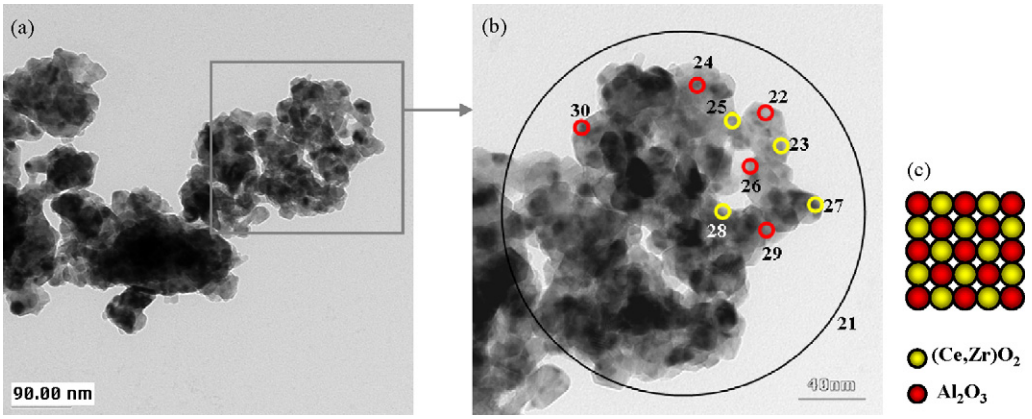

Fig. 8. TEM image of ACZ after heat treatment at 1000 °C in air for (a) low magnification, (b) large magnification for square frame in image (a), and (c) the model of secondary particles of ACZ.

(2 wt%) on CZ, CZ + Al_2O_3 and ACZ. The OSC-c1 of PtCZ(F) was higher than those of Pt(CZ + Al_2O_3) and PtACZ(F). After durability testing at 1000 °C, the OSC-c1 of each catalyst decreased to about 70% of the corresponding fresh catalyst, and the order in which the OSC-c1 of PtCZ(F) was higher than those of Pt(CZ + Al_2O_3) and PtACZ(F) was the same as in the case of the fresh catalyst.

Moreover, the OSC-c1 of PtCZ(P) was almost equivalent to that of PtCZ(A) (Fig. 9 and Table 9). Similarly, the OSC-c1 of Pt(CZ + Al_2O_3) and PtACZ(P) showed almost the same value as those of corresponding catalysts(A).

The OSC-c1 of the fresh catalysts, PtCZ(F) and PtACZ(F), evaluated using the flow-type reaction apparatus is shown in Fig. 10. Each OSC-c1 of PtCZ(F) and PtACZ(F) measured using the flow-type reactor was almost equivalent to the value of the corresponding catalyst measured using the thermogravimetric analyzer.

Figs. 11 and 12, and Table 9 shows the OSC-c2 of each catalyst. The OSC-c2 was derived from the OSC-c1, which is the molar ratio of released oxygen molecules to cerium atoms at each measurement temperature with a maximum value of 0.25 [20]. The OSC-c2 values of the Pt loaded ACZ were equal to or more than those of Pt loaded CZ and CZ + Al_2O_3. This result shows that the releasing efficiency of oxygen molecules per unit cerium is higher in ACZ than that in CZ.

3.5.2. Oxygen release rate (OSC-r)

The oxygen release rate of the catalysts after each heat treatment is shown in Fig. 13. In fresh catalysts, the oxygen release rate of PtACZ(F) was about 1.8 times higher than that of PtCZ(F) and about 1.3 times higher than that of Pt(CZ + Al_2O_3)(F).

After durability testing at 1000 °C, the OSC-r of each catalyst decreased significantly. In particular, the OSC-r of PtCZ(A) and Pt(CZ + Al_2O_3)(A) remarkably decreased to about one-fortieth in this test. PtACZ(A) showed a release

Table 6
EDX analysis results of CZ

No.	Atom%	
	Ce	Zr
21	52.8	47.2
22	39.3	60.7
23	37.6	62.4
24	53.4	46.6
25	35.4	64.6
26	40.5	59.5
27	42.2	57.8
28	42.9	57.1
29	55.1	44.9
30	43	57
31	45.1	54.9
32	43.3	56.7
33	38.4	61.6
34	37.2	62.8
35	39.9	60.1
36	40.3	59.7

Table 7
EDX analysis results of CZ + Al_2O_3

No.	Atom%		
	Al	Ce	Zr
1	98.6	0.6	0.7
2	17.2	40.0	42.8

Table 8
EDX analysis results of ACZ

No.	Atom%		
	Al	Ce	Zr
21	10.8	42.0	47.2
22	41.2	18.8	40.0
23	8.1	57.9	34.0
24	45.8	15.6	38.6
25	5.4	59.3	35.3
26	25.7	25.4	48.9
27	8.5	52.7	38.8
28	8.5	25.6	65.9
29	18.3	27.0	54.8
30	24.9	20.3	54.8

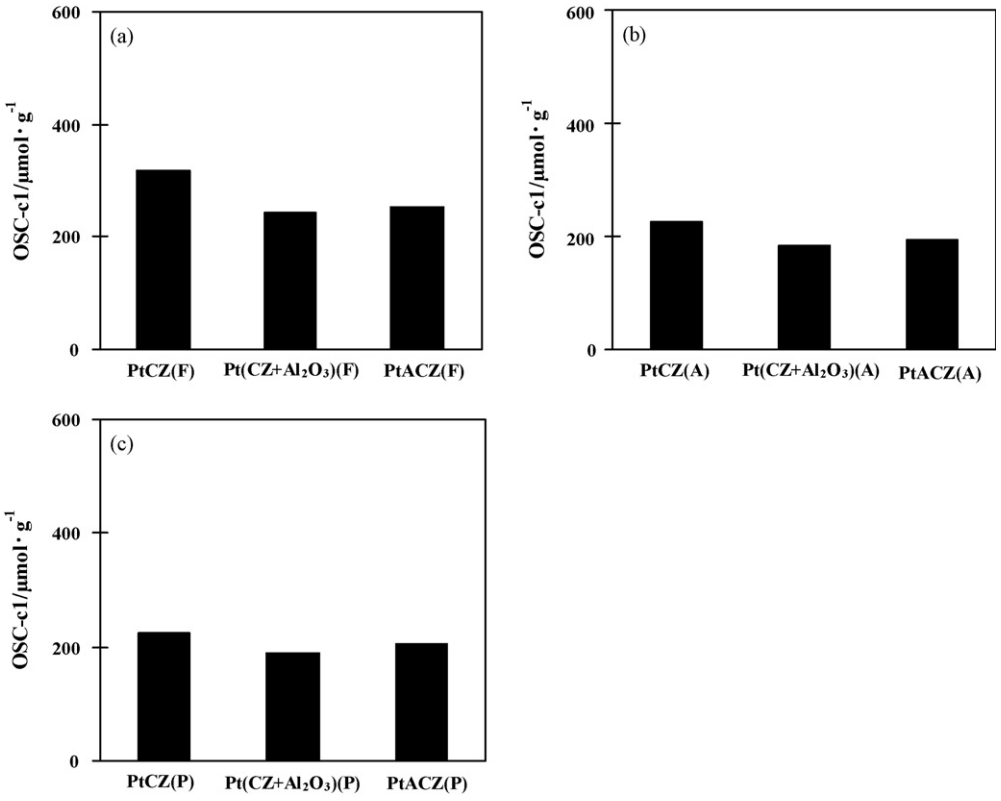

Fig. 9. OSC-c1 of catalyst after various heat treatments (a) fresh, (b) after durability test at 1000 °C, and (c) support heated at 1000 °C in air before Pt loading.

rate about four times larger than those of PtCZ(A) and Pt(CZ + Al_2O_3)(A). The decrease in the OSC-r of PtACZ(P), Pt(CZ + Al_2O_3)(F) and PtCZ(P) compared to each fresh catalyst was relatively smaller than those of corresponding catalysts(A).

In particular, the degradation of the OSC-r of PtACZ(A) was more restricted and smaller than those of PtCZ(A) and Pt(CZ + Al_2O_3)(A). The order of OSC-r between ACZ, CZ + Al_2O_3 and CZ catalysts did not change for all heat treatments.

3.5.3. Mean size of Pt particles

The mean size of Pt particles in the catalysts after each heat treatment was measured using the CO pulse adsorbing method as shown in Table 9. In fresh catalysts, Pt particles on PtACZ(F) and Pt(CZ + Al_2O_3)(F) had a diameter of 0.7 and 0.8 nm, respectively, which were almost one-half of the size of Pt particles in PtCZ(F).

After durability testing at 1000 °C, the size of Pt particles on ACZ (PtACZ(A)) was 24.8 nm, which was about 70 and 80% of the size of Pt particles on PtCZ(A) and Pt(CZ + Al_2O_3)(A).

Table 9
Collection of various OSC and Pt, $(Ce,Zr)O_2$ crystallite size

	OSC-c1 (μmol/g (cat))	OSC-c2 (mol/mol (CeO_2))	OSC-r (μmol/g(cat)·s)	Pt[a] (nm)	$(Ce,Zr)O_2$[b] (nm)
PtCZ(F)	317	0.102	13.1	1.2	8.4
PtCZ(A)	225	0.073	0.3	35.0	19.6
PtCZ(P)	225	0.073	0.5	2.6	19.6
PtCZ(flow)	277	0.090	–	–	–
Pt(CZ + Al_2O_3)(F)	242	0.106	16.1	0.8	6.7
Pt(CZ + Al_2O_3)(A)	185	0.081	0.4	29.7	18.7
Pt(CZ + Al_2O_3)(P)	190	0.083	1.5	2.2	18.7
PtACZ(F)	252	0.110	20.3	0.7	6.4
PtACZ(A)	192	0.084	1.4	24.8	9.7
PtACZ(P)	204	0.089	7.0	2.2	9.7
PtACZ(flow)	255	0.111	–	–	–

(F) fresh catalysts, (A) catalysts aged at 1000 °C in air, (P) catalyst supports pre-heated at 1000 °C in air before Pt loading.
[a] Measured by CO pulse adsorption method at about −70 °C.
[b] Measured by XRD.

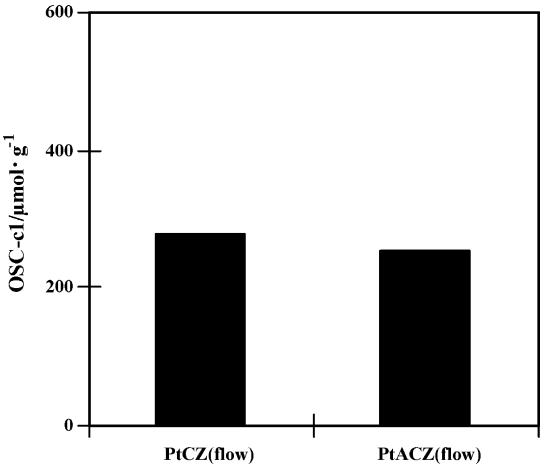

Fig. 10. OSC-c1 of fresh catalysts evaluated by the flow system.

A significant difference among three catalysts(P) was not observed when supports were only heated at 1000 °C before loading Pt. However, the Pt particles in each catalyst became slightly larger than those in the fresh catalysts. Generally, the specific surface area of a catalyst support affects the mean diameter of loaded Pt particles on the fresh catalyst. 1 wt% of Pt needs more than 30 m^2/g of specific surface area of a catalyst support for sufficient dispersion of fine particles around 0.7 nm [21]. The larger size of Pt particles in PtCZ(P), Pt(CZ + A-l_2O_3)(P) and PtACZ(P) than that in the corresponding fresh catalysts was because of their insufficient surface area for this concentration of Pt.

3.5.4. Conclusion of OSC characteristics

The OSC-c1 values evaluated by the thermogravimetric analyzer and the flow-type reactor were almost equivalent. This result confirms the validity and reliability of both appraisal methods for the OSC-c1.

The OSC-c1 of PtCZ(F) exceeded that of PtACZ(F), which was almost the same as that of Pt(CZ + Al_2O_3)(F), and the value of PtCZ(F) was about 1.3 times the PtACZ(F) per unit weight because of the larger concentration of (Ce,Zr)O_2. PtCZ(F) contained 3.4 mmol CeO_2 in 1 g of catalyst, which was about 1.4 times that of PtACZ(F) and Pt(CZ + Al_2O_3)(F) (both containing 2.5 mmol CeO_2 per gram). The particle sizes of (Ce,Zr)O_2 in all three catalysts(F) were almost equal and the Pt particle size of PtACZ(F) (0.7 nm) was smaller than that of PtCZ(F) (1.2 nm) and almost equal to that of Pt(CZ + A-l_2O_3)(F) (0.8 nm); however, the OSC-c2 of all three catalysts(F) were almost the same (Table 9 and Fig. 11). In other words, the bottleneck of OSC-c1 and OSC-c2 was not Pt particle size. The OSC-c2 was defined as the molar ratio of the released oxygen to all oxygen corresponding to the chemically equivalent concentration of Ce cations. This result reveals the reaction efficiencies of CeO_2 in fresh catalyst at each measured temperature in this condition.

After durability testing at 1000 °C in air, the OSC-c1 and OSC-c2 of PtCZ(A) were equal to the corresponding values of PtCZ(P), which were about 70% of PtCZ(F). Similarly, the OSC-c1 and OSC-c2 of PtACZ(A) and Pt(CZ + Al_2O_3)(A) showed almost the same values as those of OSC-c1 and OSC-c2 of the corresponding catalysts(P). Pt particle sizes in aged

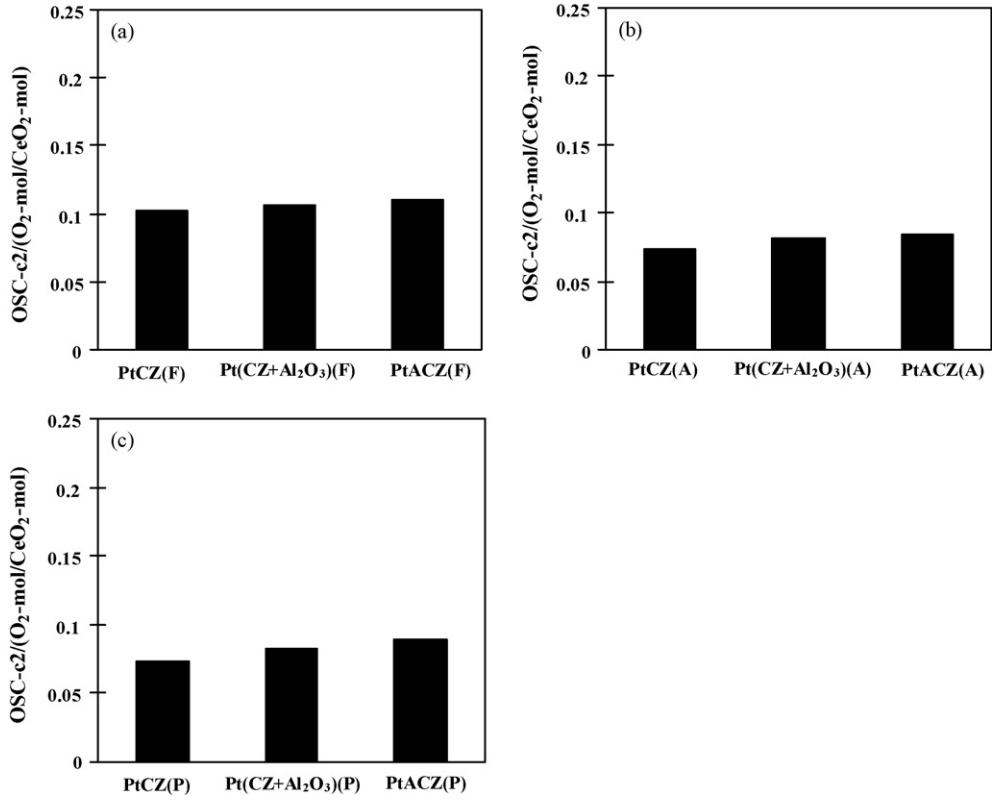

Fig. 11. OSC-c2 of catalysts after various heat treatments (a) fresh, (b) after durability test at 1000 °C, and (c) support heated at 1000 °C in air before Pt loading.

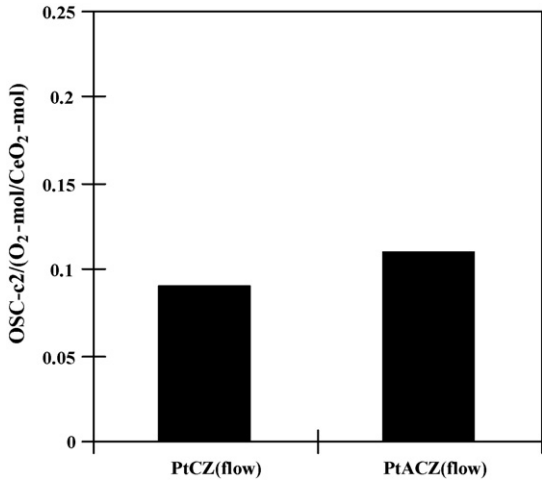

Fig. 12. OSC-c2 of fresh catalysts evaluated by the flow system.

catalysts(A) (35.0 nm in PtCZ(A), 29.7 nm in Pt(CZ + A-l_2O_3)(A) and 24.8 nm in PtACZ(A)) were much larger than those of corresponding catalysts(P) that were loaded with Pt after pre-heating CZ and ACZ at 1000 °C. Pt particle size of PtCZ(P) was 2.6 nm and those of both PtACZ(P) and Pt(CZ + Al_2O_3)(F) were 2.2 nm. These results suggest that the OSC-c1 and OSC-c2 values measured with the thermo-gravimetric analyzer are hardly affected by Pt particle size within 10 times of their size if measurement time is sufficiently long to diffuse oxygen both in bulk and on surface to reach a saturation level. For this reason, the OSC-c2 of the three fresh catalysts, PtCZ(F), Pt(CZ + Al_2O_3)(F) and PtACZ(F), were almost equal. In addition, the OSC-c2 of PtACZ(P) and PtACZ(A), in which the sintering of (Ce,Zr)O_2 after heat treatment was suppressed by the Al_2O_3 diffusion barrier, showed slightly higher values than those of the corresponding Pt loaded CZ and CZ + Al_2O_3 catalysts.

The oxygen releasing processes consist of the following two steps. One step is oxygen transfer on the surface of the (Ce,Zr)O_2 particles, and the other is oxygen volume diffusion inside the particles [22,23].

Generally, if the particle size of (Ce,Zr)O_2 is large enough, the volume diffusion rate has a larger influence on OSC-r than the surface diffusion rate [22,23]. Furthermore, the size and level of dispersion of Pt fine particles that are used for oxygen release and CO adsorption are also important.

In the fresh catalysts, the OSC-r of PtACZ(F) was about twice as fast as that of PtCZ(F). The (Ce,Zr)O_2 particle sizes in the two catalysts were almost equal and the Pt particle size in PtACZ(F) was about one-half of the Pt particle size in PtCZ(F); in other words, the numbers of activation sites of CO or O_2 in PtACZ(F) were twice that in PtCZ(F). This means that the finer Pt particles in PtACZ(F) promote the OSC-r more than the coarser ones in PtCZ(F); in other words, the dominant factor for the difference of the OSC-r between PtCZ(F) and PtACZ(F) is Pt particle size. On the other hand, the OSC-r of Pt(CZ + Al_2O_3)(F), which had almost same size Pt particles, was three-quarters that of PtACZ(F). The crystallite sizes of (Ce,Zr)O_2 of both Pt(CZ + A-l_2O_3)(F) and PtACZ(F) were almost equal. Pt particles of both catalysts were dispersed on the catalyst supports; however, the distribution of Al_2O_3 and (Ce,Zr)O_2 of CZ + Al_2O_3 was not uniform in comparison with that of ACZ, as shown in Figs. 7 and

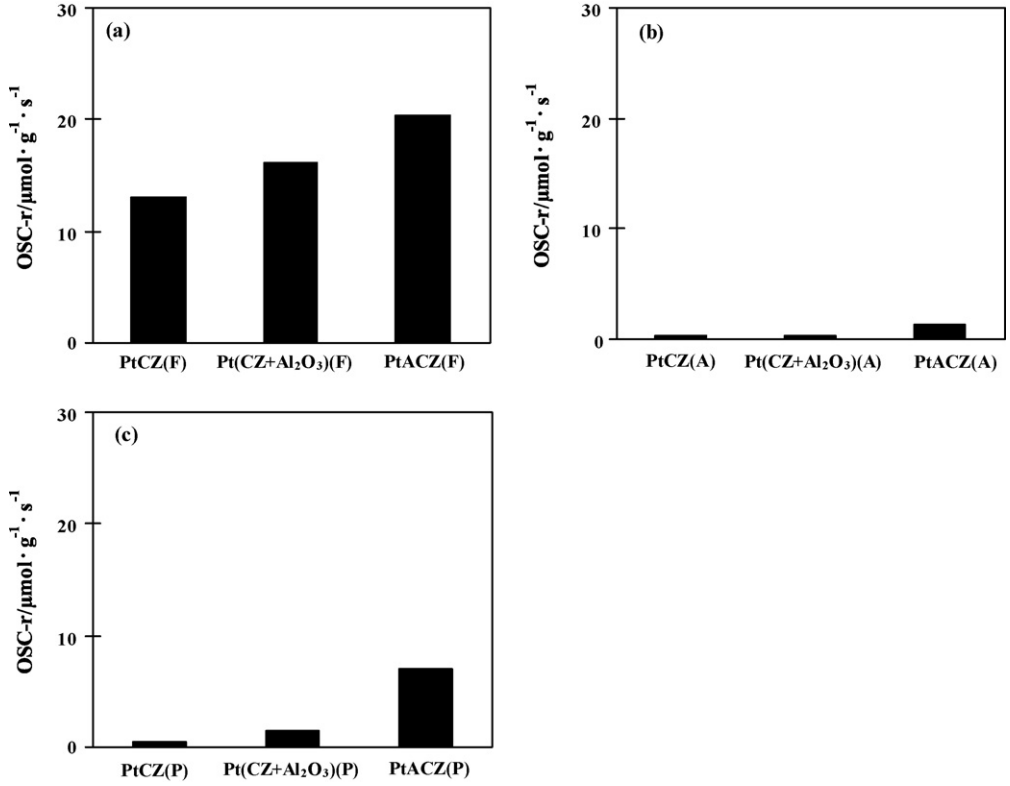

Fig. 13. OSC-r of catalysts after various heat treatments (a) fresh, (b) after durability test at 1000 °C, and (c) support heated at 1000 °C in air before Pt loading.

8. Therefore, the distance between Pt and $(Ce,Zr)O_2$ particles could be farther than that of PtACZ(F). As a result, the OSC-r of $Pt(CZ + Al_2O_3)(F)$ was smaller than that of PtACZ(F).

In the case of catalysts loaded with Pt after pre-heating of supports, the OSC-r of PtCZ(P) and $Pt(CZ + Al_2O_3)(P)$ decreased to less than one-tenth of those of corresponding catalysts(F). On the other hand, degradation of the OSC-r of PtACZ(P) was restricted and the value was about one-third of that of PtACZ(F). The sizes of Pt particles in both $Pt(CZ + Al_2O_3)(P)$ and PtACZ(P) were equal (2.2 nm, Table 9), but the $(Ce,Zr)O_2$ particle size of $Pt(CZ + Al_2O_3)(P)$ (about 20 nm) was twice as large as that of PtACZ(P) (about 10 nm), suggesting that the OSC-r depends on the size of $(Ce,Zr)O_2$ in supports because of the difference of the distance between Pt and $(Ce,Zr)O_2$ particles. Additionally, the OSC-r of PtCZ(P), on which the $(Ce,Zr)O_2$ particle size was equal to that of $Pt(CZ + Al_2O_3)(P)$ (each size was 20 nm, Table 9), was one-third of that of $Pt(CZ + Al_2O_3)(P)$ and the particle size of Pt in $Pt(CZ + Al_2O_3)(P)$ was slight smaller than that in PtCZ(P). These results also suggest that Pt particle size affects the OSC-r of catalysts.

After durability testing at 1000 °C in air, both Pt and $(Ce,Zr)O_2$ particles sintered remarkably in PtCZ(A). The size of Pt particles was about 35 nm, which was about 14 times larger than that in PtCZ(P); however, the size of $(Ce,Zr)O_2$ in PtCZ(A) was almost the same as that in PtCZ(P). Besides, in case of $Pt(CZ + Al_2O_3)$, almost the same change of both Pt particle size and $(Ce,Zr)O_2$ particle size was observed. On the other hand, Pt particles also grew considerably in PtACZ(A) and the size was about 25 nm, which was about 12 times larger than that of PtACZ(P); however, the particle sizes of $(Ce,Zr)O_2$ in these catalysts were almost the same. The OSC-r of all three catalysts(A) degraded significantly more than those of the corresponding catalysts loaded with Pt after pre-heating of supports. This result indicates that the OSC-r remarkably decreased by sintering of Pt particles. It should not be overlook the fact that the OSC-r of PtACZ(A) was four times larger than those of the other two catalysts could indicate the suppression effect of $(Ce,Zr)O_2$ by the Al_2O_3 diffusion barrier.

Therefore, it became apparent that the grain growth of both Pt and $(Ce,Zr)O_2$ influenced the OSC-r of catalysts in spite of their heating history. This differed from the case of OSC-c1 and OSC-c2. The Al_2O_3 diffusion barrier suppressed the particle growth of $(Ce,Zr)O_2$ and Pt, which led to larger OSC-r of the Pt loaded ACZ catalysts compared with those of Pt loaded CZ or $CZ + Al_2O_3$ catalysts.

From the above mentioned results, the following mechanism can be shown. The particle growth of $(Ce,Zr)O_2$ was inhibited by introducing Al_2O_3 components mixed with $(Ce,Zr)O_2$ at the nanometer scale, and the introduction of the Al_2O_3 diffusion barrier simultaneously achieved the improvement in oxygen release rate in fresh catalyst and inhibition of degradation of the rate after durability testing.

4. Conclusions

(1) In ACZ, the Al_2O_3 diffusion barrier introduced at the nanometer scale among $(Ce,Zr)O_2$ primary particles inhibited the growth of $(Ce,Zr)O_2$ during durability testing up to 1000 °C.
(2) The decrease in the specific surface area of ACZ was suppressed as a result of particle growth inhibition of $(Ce,Zr)O_2$ by not the Al_2O_3 introduced at the submicron scale but the Al_2O_3 diffusion barrier at the nanometer scale.
(3) The saturated OSC (OSC-c1 and OSC-c2) of Pt loaded ACZ, $CZ + Al_2O_3$ and CZ in fresh catalyst and that after durability testing were hardly affected by the particle sizes of Pt and $(Ce,Zr)O_2$.
(4) The oxygen release rate (OSC-r) of Pt loaded ACZ, $CZ + Al_2O_3$ and CZ was closely related to the size of both Pt and $(Ce,Zr)O_2$ particles. The OSC-r of catalysts(F) advanced by the Al_2O_3 diffusion barrier, which was introduced into $(Ce,Zr)O_2$ not at the sub-micron scale but at the nanometer scale. After durability testing, the Pt loaded ACZ inhibited the particle growth of $(Ce,Zr)O_2$ because of the Al_2O_3 diffusion barrier, and restricted the reduction in the specific surface area. Hence, the growth of Pt particles was inhibited and the distance between Pt and $(Ce,Zr)O_2$ could be kept closely. As a result, the Pt loaded ACZ maintained larger OSC-r than that of Pt loaded CZ or $CZ + Al_2O_3$.

Acknowledgement

The authors would like to thank the members of the Catalyst Laboratory of TOYOTA R&D RABS., INC.

References

[1] S. Matsumoto, Toyota Tec. Rev. 44 (1994) 10.
[2] H.S. Gandhi, A.G. Piken, M. Shelef, R.G. Delesh, SAE Paper 760201 (1976).
[3] H.C. Yao, Y.F. Yu Yao, J. Catal. 86 (1984) 254.
[4] T. Kanazawa, J. Suzuki, T. Takada, T. Suzuki, A. Morikawa, A. Suda, H. Sobukawa, M. Sugiura, SAE Paper No. 2003-01-0811 (2003).
[5] An Open Patent Official Report and Provisional Publication No. 63-116741 (1988).
[6] S. Matsumoto, N. Miyoshi, T. Kanazawa, M. Kimura, M. Ozawa, in: S. Yoshida, N. Tabezawa, T. Ono (Eds.), Catalysis Science and Technology, vol. 1, Kodansha/VCH, Tokyo/Weinheim, 1991, p. 335.
[7] M. Ozawa, M. Kimura, A. Isogai, J. Alloys Comp. 193 (1993) 73.
[8] A. Suda, T. Kandori, Y. Ukyo, H. Sobukawa, M. Sugiura, J. Ceram. Soc. Jpn. 108 (2000) 473.
[9] A. Suda, H. Sobukawa, T. Suzuki, T. Kandori, Y. Ukyo, M. Sugiura, J. Ceram. Soc. Jpn. 109 (2001) 177.
[10] A. Suda, H. Sobukawa, T. Suzuki, T. Kandori, Y. Ukyo, M. Sugiura, J. Ceram. Soc. Jpn. 110 (2002) 126.
[11] J. Kaspar, P. Fornasiero, N. Hickey, Catal. Today 77 (2003) 419.
[12] Reference Catalyst Committee, Catalysis Society of Japan, Catalysis & Catalysts 28 (1986) 41.
[13] Reference Catalyst Committee, Catalysis Society of Japan, Catalysis & Catalysts 31 (1989) 317.
[14] An Open Patent Official Report and Provisional Publication No. 2004-340637.
[15] A. Suda, K. Yamamura, Y. Ukyo, T. Sasaki, H. Sobukawa, T. Tanabe, Y. Nagai, M. Sugiura, J Ceram. Soc. Jpn. 112 (2004) 623.
[16] T. Tanabe, A. Suda, C. Desorme, D. Duprez, H. Shinjyoh, M. Sugiura, Stud. Sci. Catal. 138 (2001) 135.
[17] J. Kaspar, P. Fornasiero, Catal. Today 50 (1999) 285.
[18] S.J. Wilson, G.D. McConneil, J. Solid State Chem. 34 (1980) 315.

[19] L. Pach, R. Roy, S. Komarneni, J. Mater. Res. 5 (1990) 278.
[20] Y. Nagai, T. Yamamoto, T. Tanaka, S. Yoshida, T. Nonaka, T. Okamoto, A. Suda, M. Sugiura, Catal. Today 74 (2002) 225.
[21] A. Suda, K. Yamamura, Y. Ukyo, T. Sasaki, H. Sobukawa, T. Tanabe, Y. Nagai, M. Sugiura, J Ceram. Soc. Jpn. 112 (2004) 581.
[22] F. Dong, A. Suda, T. Tanabe, Y. Nagai, H. Sobukawa, H. Shinjoh, M. Sugiura, C. Descorme, D. Duprez, Catal. Today 93–95 (2004) 827.
[23] F. Dong, A. Suda, T. Tanabe, Y. Nagai, H. Sobukawa, H. Shinjoh, M. Sugiura, C. Descorme, D. Duprez, Catal. Today 90 (2004) 223.
[24] T. Kanazawa, Catal. Today 96 (2004) 171.
[25] T. Kanazawa, J. Suzuki, T. Takada, T. Suzuki, A. Morikawa, A. Suda, H. Sobukawa, M. Sugiura, Science and Technology in Catalysis 200, Kodansha Elsevier, 2003,, p. 185.
[26] M. Yashima, S. Sasaki, Y. Yamaguchi, M. Kakihana, M. Yoshimura, T. Mori, Appl. Phys. Lett. 72 (1998) 182.